Journal of Electronic Materials (2022) 51:4139–4144
https://doi.org/10.1007/s11664-022-09710-8

MAGNETIC OXIDES

Structural, Electronic, and Magnetic Properties of $NiGa_2O_4$

Aditya Sharma[1] · Mayora Varshney[2] · Yogesh Kumar[3] · Ankush Vij[4] · Ram K. Sharma[5] · Hyun-Joon Shin[6]

Received: 26 February 2022 / Accepted: 9 May 2022 / Published online: 7 June 2022

Abstract
In this study, $NiGa_2O_4$ phase is prepared using a sonication-assisted hydrothermal method. Rietveld-fitted x-ray diffraction results reveal the formation of a single-phase compound with average crystallite size of ~32.5 nm. UV-visible absorption spectroscopy results show bandgap energy of 4.1 eV. X-ray absorption near-edge structural analysis confirms the presence of Ga^{3+} and Ni^{2+} ions in Ga_2NiO_4. The magnetic properties of $NiGa_2O_4$ phase are studied at two temperatures (i.e., 50 K and 300 K), and the $NiGa_2O_4$ phase is found to be paramagnetic. The origin of magnetism in the $NiGa_2O_4$ phase is mechanistically discussed by considering the plausible magnetic interactions among the constituent ions in the compound.

Keywords Ga_2NiO_4 · magnetism · XANES

Introduction

The AB_2O_4 spinel oxides are attractive compounds exhibiting diverse properties because of multifaceted interactions among the constituent cations of different sizes and variable valence states. AB_2O_4 compounds have also been reported with catalytic, light emission, gas-sensing, and magnetic properties.[1–6] Based on the distribution of cations at octahedral and tetrahedral sites, the AB_2O_4 spinel oxides can be divided into two broad categories, and the AB_2O_4 formula unit can be written in terms of the degree of inversion parameter (x) as $\{A_{1-x}B_x\}[B_{2-x}A_x]O_4$. In this formula unit, the cations in the curly brackets and square brackets represent the tetrahedral and octahedral sites, respectively.[7,8] For the normal spinels (with $x = 0$, in the above formula unit), the cubic symmetry (Fd-3m) provides octahedral sites to the B element and tetrahedral sites to the A element. On the other hand, the inverse spinels (with $x = 1$) consist of all of the A cations and half of the B cations at octahedral sites, and the remaining half of the B cations occupy the tetrahedral sites. Other hybrid spinels can also be prepared with the $0 < x < 1$ configuration; however, they are high-temperature phases and known as disordered-dual spinel phases.[9,10] Among all AB_2O_4 compounds, gallate spinels have attracted particular attention.[11,12] Some of the transition metal-containing $MgGa_2O_4$ spinels exhibit absorption and luminescence properties useful for optoelectronic devices.[13] Nickel gallates have also been found to be a potential catalyst for NO reduction as well as for the photocatalytic dissociation of water.[14,15] $NiGa_2O_4$ has also found application in supercapacitors, gas sensors, and glucose sensors.[16–18]

Various synthesis approaches have been established to grow nickel gallates;[19,20] however, the distribution of constituent cations (at tetrahedral/octahedral sites) largely depends on the operating temperatures and other synthesis protocols. A slight variation in the site occupancy of an element (driven by synthesis protocols) may facilitate diverse hybridization of frontier orbitals and, consequently, a variety of electronic structural and magnetic

✉ Aditya Sharma
adityaiuac@gmail.com

Hyun-Joon Shin
shin@chungbuk.ac.kr

1 Department of Physics, Manav Rachna University, Faridabad, Haryana 124001, India

2 Department of Applied Physics, School of Vocational and Applied Sciences, Gautam Buddha University, Greater Noida, Uttar Pradesh 201312, India

3 Solid State Physics Division, Bhabha Atomic Research Centre, Mumbai 400085, India

4 Department of Physics, University of Petroleum and Energy Studies, Dehradun, Uttarakhand 248007, India

5 Centre for Interdisciplinary Research and Innovation, University of Petroleum and Energy Studies, Dehradun 248007, India

6 Department of Physics, Chungbuk National University, Cheongju 28644, South Korea

properties in the compounds. For the case of the $NiGa_2O_4$ compound, the relationship between the electronic structure and magnetic properties is not significantly reported in the literature. In this study, $NiGa_2O_4$ nanocrystals are prepared using a sonication-assisted hydrothermal method. The crystal structure and lattice parameters of $NiGa_2O_4$ are investigated using x-ray diffraction (XRD) and Rietveld refinement. Hybridization of frontier orbitals and electronic structural properties are studied using x-ray absorption near-edge structure (XANES) spectroscopy at the O K-, Ni K-, and Ga K-edge. The low-temperature (50 K) and room-temperature magnetic properties of $NiGa_2O_4$ nanoparticles are also investigated and mechanistically discussed by considering the magnetic interactions among the constituent cations.

Experimental

The pure $NiGa_2O_4$ phase was synthesized by the wet chemical method. All the reagents used were of analytical grade without further purification. One gram of $Ga(NO_3)_3$ and 1 g of $C_4H_6NiO_4.4H_2O$ (nickel (II) acetate tetrahydrate) were separately dissolved in 200 ml ethanol and stirred (100 rpm) for 1 h. The solutions were poured into another beaker and stirred (200 rpm) for 30 min followed by sonication for 30 min. Next, 10 mol ethyl glycol (20 ml) was added to the above-prepared solution, and the final dense solution was heated at 80°C in an oven. The as-dried powder was annealed at 1150°C for 4 hours. The cooling steps were kept the same as the temperature gradient heating steps (with a heating/cooling rate of 15°C/min). XRD measurements were performed using Cu Kα radiation with a wavelength of 1.5418 Å. The Bruker D8 Advance diffractometer, operated at 40 kV accelerating voltage and 40 mA tube current, was used in this work. During data collection, the scan speed was 1°/min in steps of 0.02°. The XRD data were analyzed with Rietveld refinement using FullProf software. O K-edge XANES spectra were collected in total electron yield (TEY) mode at the soft x-ray beamline (10D-XAS-KIST) of the Pohang Accelerator Laboratory (PAL), South Korea. The photon energy resolution of this beamline was better than 0.6 eV (at the O K-edge). Ni K-edge and Ga K-edge XANES spectra were collected from the x-ray scattering beamline (1D XRS KIST-PAL) of PAL, South Korea. The data collection procedure and uses of gas mixtures and typical procedures for the background removal and normalization are provided elsewhere.[21] Low-temperature (50 K) and room-temperature (300 K) magnetization measurements were performed using the commercial Quantum Design Physical Property Measurement System (PPMS).

Results and Discussion

Figure 1 shows the XRD pattern for the $NiGa_2O_4$ compound along with the Rietveld refinement curve, Bragg's peak positions, and difference line. The XRD pattern was refined with a cubic unit cell (space group Fd-3m). Good agreement is observed between the calculated and experimental XRD patterns, evidenced by the almost flat, straight difference line in Fig. 1. There are no traces of other phases (e.g., Ga_2O_3, NiO) in the XRD patterns, indicating the single-phase formation of $NiGa_2O_4$ by applying the given synthesis protocols. The calculated lattice parameters, Wyckoff positions, and other fitting parameters are listed in Table I. A comparison of lattice parameters, space group, and Wyckoff positions of the $NiGa_2O_4$, Ga_3O_2, and NiO[22] compounds is also tabulated in Table I. The distinct difference in the lattice parameters and Wyckoff positions of the three compounds indicates dissimilarity in their crystal structures and space groups. The average crystallite size of $NiGa_2O_4$ is calculated using the Scherrer relation $D = 0.9\lambda/(\beta\cos\theta)$, where β is the full width at half-maximum of the peaks. The estimated crystallite size is ~32.5 nm.

Figure 2 shows the UV-visible absorption spectra of $NiGa_2O_4$ in the range of 200–600 nm range. A clear absorption peak is observed at 270 nm. The inset of Fig. 2 shows the Tauc plot [i.e., graph of $(\alpha h\upsilon)^2$ versus photon energy $(h\upsilon)$]. The bandgap energy is estimated by finding an

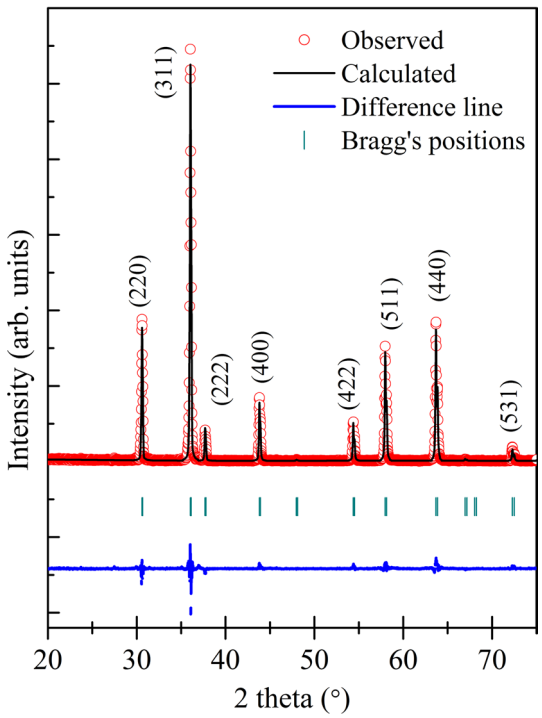

Fig. 1 Rietveld-refined XRD patterns of $NiGa_2O_4$.

Table I Lattice parameters, Wyckoff positions, and Rietveld-refined parameters of NiO, β-Ga_2O_3 and $NiGa_2O_4$

Sample name	Lattice parameters		Wyckoff positions					Fitting parameters
$NiGa_2O_4$	$a = b = c =$ 8.25895 Å (Space group; Fd-3m)	$\alpha = \beta = \gamma$ =90°	O $x = y = z =$ 0.25465(68)	Ni_1 $x = y = z =$ 0.12500 (0)	Ga_1 $x = y = z =$ 0.12500 (0)	Ni_2 x = y = z = 0.50000 (0)	Ga_2 x=y=z= 0.50000 (0)	$\chi^2 = 1.89$ $R_{wp} = 20.2$
NiO Ref. [22]	$a = b = c =$ 4.186 Å (Space group; Fm-3m)	α =β = γ =90°	O $x = y = z =$ 0.50000 (0)	Ni_1 $x = y = z$ = 0.00000				Not reported
Ga_2O_3 Ref. [25]	$a =$ 12.2169(19), $b =$ 3.0392(4), $c =$ 5.8095(8) (Space group; C^2/m)	$\alpha = \gamma = 90°$, β = 103.81°	O_1 x= 0.15223 y= 0.00000 z= 0.52278	O_2 $x = 0.20188$ $y = 0.00000$ $z = 0.21165$	O_3 $x = 0.51348$ $y = 0.00000$ $z = 0.11035$	Ga_1 $x = 0.08249$ $y = 0.00000$ $z = 0.32215$	Ga_2 x= 0.34215 y= 0.00000 z = 0.19608	$\chi^2 = 1.4$ $R_{wp} = 10.4$

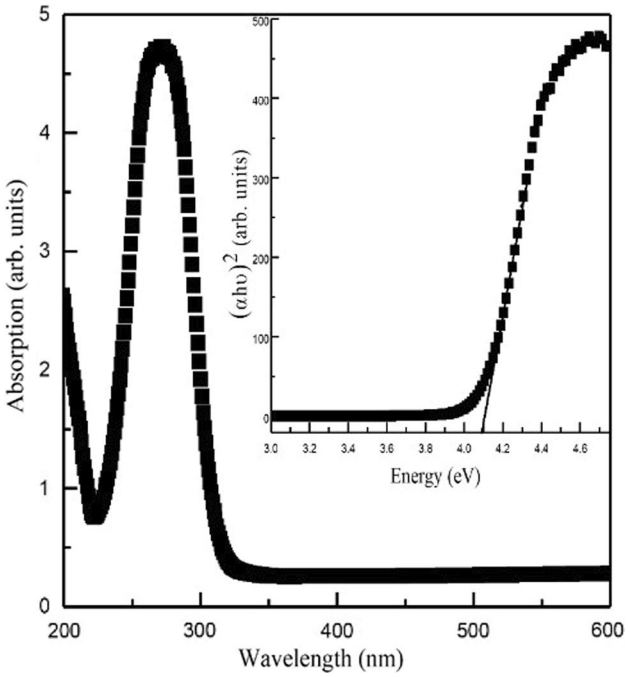

Fig. 2 The UV-visible absorption spectrum of the $NiGa_2O_4$ compound. Inset shows the determination of bandgap energy.

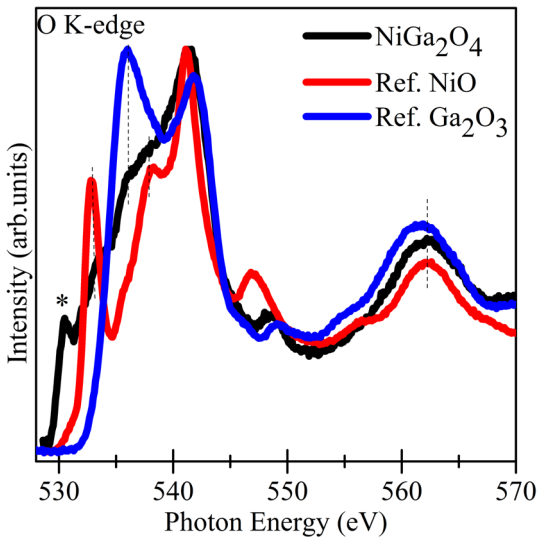

Fig. 3 O K-edge XANES spectra of $NiGa_2O_4$ along with reference NiO and β-Ga_2O_3.

intersection to the energy axis by extrapolating the linear portion of the *y*-axis. The calculated bandgap energy of the $NiGa_2O_4$ compound is ~ 4.1 eV.

Figure 3 shows the feature-rich O K-edge spectra from the Ga_2O_3, NiO, and $NiGa_2O_4$ compounds. In the case of the O K-edge XANES, the O 1s electrons transition to the empty or hybridized 2p orbitals. In the case of transition metal oxides, there are four types of well-defined partially occupied and unoccupied molecular orbitals. These molecular orbitals, and the corresponding atomic orbitals that contribute dominantly to the molecular orbitals, are in qualitative energetic order of $2t_{2g}$ (M 3d; O $2p_\pi$) < $3e_g$ (M 3d; O $2p_\sigma$) < $3a_{1g}$ (M 4s; O $2p_\sigma$) < $4t_{1u}$ (M 4p; O $2p_\pi$), where M represent the transition metal element.[23,24] The transition of ls electrons to all four molecular orbitals is dipole-allowed because of the presence of the p-character in these hybridized orbitals.[23,24] A simple molecular orbital theory can be used to understand the main differences in the O K-edge features of various transition metal oxides (Fig. 4).

In the case of NiO (i.e., Ni^{2+}, with $3d^8$ electronic configuration), the $2t_{2g}$ orbitals (i.e., group of d_{xy}, d_{xz}, and d_{yz} orbitals, with 6 electrons) are completely occupied, and the degenerate $3e_g$ orbitals (i.e., group of d_z^2 and $d_{x^2-y^2}$ orbitals, with 2 electrons) are partially occupied. A sharp O

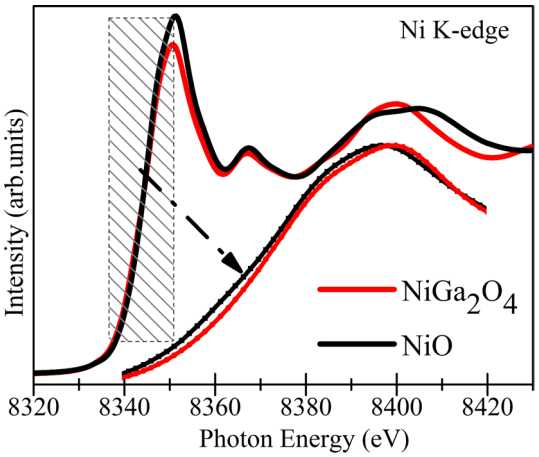

Fig. 4 Ni-edge XANES spectra of $NiGa_2O_4$ and NiO.

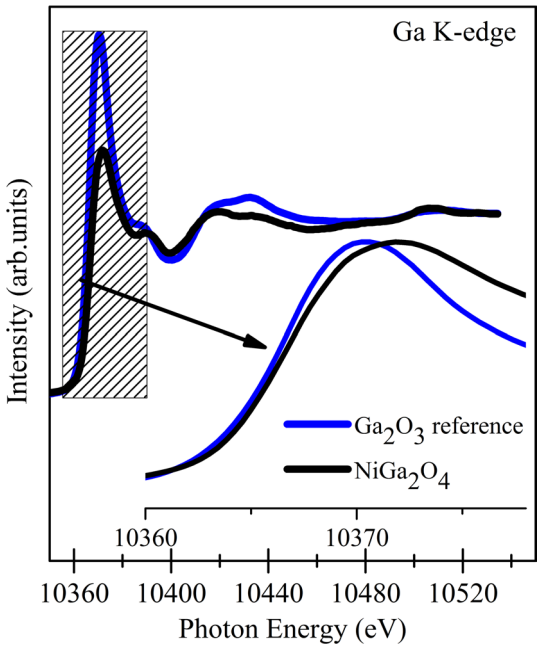

Fig. 5 Ga K-edge XANES spectra of $NiGa_2O_4$ and β-Ga_2O_3.

K-edge feature (~ 532.9 eV) in NiO can be assigned to the O 1s electronic transition to the $3e_g$ orbitals.[23] The other higher-energy features (between 535 eV and 550 eV) are the electronic transition from O 1s to $3a_{1g}$–$4t_{1u}$ hybridized orbitals. Other multiple scattering features are also present in the O K-edge spectra (above 560 eV) which may originate from electronic transitions from O 1s to hybridized O 2p and metal (n +1) sp orbitals.[23,24] In the case of the Ga_2O_3 compound (β-Ga_2O_3 phase is taken in the present study), the Ga 3d states are filled because of the $3d^{10}$ electronic configuration of Ga^{3+} ions. The final state corresponds to the antibonding orbitals formed by the hybridization of the O 2p states with Ga 4s and Ga 4p.[25] It can be seen from Fig. 2 that there is no pre-edge peak (between 528 eV and 532 eV) in the β-Ga_2O_3 reference sample. This is because of the fully occupied 3d orbitals of Ga^{3+} ions. There are two spectral features (between 533 eV and 543 eV) which correspond to the electronic transitions from O 1s to the mixture of O 2p and Ga 4s and Ga 4p states.[25] The O K-edge spectrum of the $NiGa_2O_4$ sample exhibits diverse spectral features. Based on previous reports, the intense pre-edge feature (530.1 eV) may be due to the Ni^{3+} ions present in the $NiGa_2O_4$ sample as observed for $NdNiO_3$ samples.[25] The O K-edge XANES for $NiGa_2O_4$ samples is not reported in the literature. Therefore, here we anticipate that the low-energy pre-edge peak in the O K-edge spectrum of the $NiGa_2O_4$ sample is due to Ni^{3+} ion-related transitions. Additionally, the other features of the $NiGa_2O_4$ sample partially match with the spectral features of the reference NiO sample. For example, the shoulder-like feature at 532.9 eV coincides with the pre-edge peak of Ni^{2+} ions containing the NiO sample and the high-energy features (at 562.2 eV) of the NiO and $NiGa_2O_4$ sample also match. This indicates that the $NiGa_2O_4$ sample is composed of Ni^{2+} and Ni^{3+} ions.

To understand the valance state of Ni in the $NiGa_2O_4$ compound, Ni K-edge XANES spectra were collected. Figure 3 presents the pre/post-edge background-subtracted and normalized Ni K-edge XANES spectra of the $NiGa_2O_4$compound. The reference sample of NiO, in which Ni ions obey the +2 valance state, was also scanned under similar experimental conditions, and the spectrum is plotted along with the spectrum of the $NiGa_2O_4$ compound. Closer examination of the spectral features (see the inset) of the XANES spectra of the NiO and $NiGa_2O_4$ samples reveals that the rising edge of the $NiGa_2O_4$ sample is at higher energy. This indicates the existence of a higher valence state of Ni ions (i.e., Ni^{3+}) in the $NiGa_2O_4$ sample. However, the main peak energy of NiO and $NiGa_2O_4$ samples is fairly coincident and suggests the presence of Ni^{2+} ions. This observation is consistent with the observations of O K-edge spectra where some of the spectral features (the pre-edge peak) were attributed to the Ni^{3+} ions and other features corresponded to the Ni^{2+} ions in the $NiGa_2O_4$ sample.

To further probe the valence state of the Ga ions in the $NiGa_2O_4$ compound and to compare the orbital hybridization with the stable oxide of Ga, the Ga K-edge XANES spectrum is collected from the reference β-Ga_2O_3 and Ga_2NiO_4. Ga obeys the 3+ valence state in the β-Ga_2O_3 compound with 50/50 percentage occupancy at tetrahedral/octahedral sites.[24,26] It has also been reported that the α-Ga_2O_3 compound, although the Ga^{3+} ions are solely present in this phase, obeys a nearly 2 eV shift in the white-line peak.[26,27] This is due to the regular octahedral occupancy of Ga^{3+} ions in the α-Ga_2O_3 compound. The normalized Ga K-edge XANES spectra are presented in Fig. 5. It can be seen that the edge-energy positions of the reference β-Ga_2O_3 and

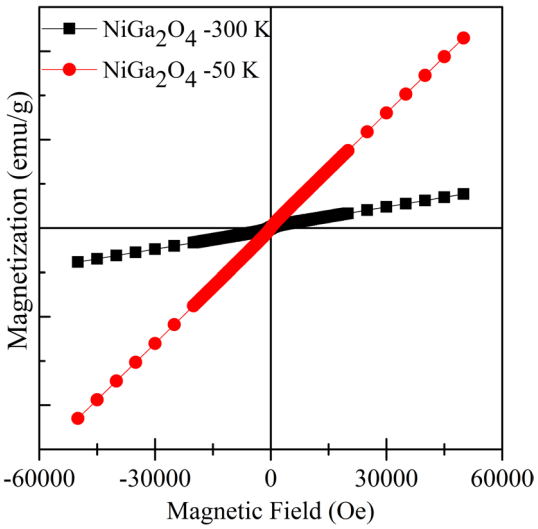

Fig. 6 Magnetic field versus magnetization data for $NiGa_2O_4$, measured at 50 K and 300 K.

$NiGa_2O_4$ samples coincide with each other, signifying the existence of Ga^{3+} ions in the $NiGa_2O_4$ sample. The broad or shifted white line peak is observed in the $NiGa_2O_4$ sample. The shifting/broadening of the white-line peak suggests noticeable octahedral occupancy by the Ga^{3+} ions in the $NiGa_2O_4$ sample.

To understand the unrevealed magnetic properties of the $NiGa_2O_4$ compound, the M-H data for the sample were collected at two different temperatures (50K and 300K). Figure 6 shows the magnetic hysteresis loop of the $NiGa_2O_4$ compound. It can be seen from Fig. 6 that the $NiGa_2O_4$ compound shows paramagnetic behavior at 50 K and 300 K. To understand the elemental origin of the magnetism, it is imperative to elucidate the cationic model of the constituent ions in the $NiGa_2O_4$ compound. As discussed in the introduction section, the $\{A_{1-x}B_x\}[B_{2-x}A_x]O_4$ cationic model may exist in the $NiGa_2O_4$ sample. In this model, the distribution and valence states of the A and B cations (with $x = 0$) can help us understand the magnetic behavior. From this model, the Ga^{3+} ions may not contribute to the net magnetization because they do not obey unpaired electrons with their fully occupied orbitals ($3d^{10}$). Therefore, only the Ni cations are expected to contribute to the observed magnetic properties. Our XANES results may help in validating the above cationic model. The Ga K-edge XANES showed the existence of octahedrally distributed Ga^{3+} ions in the $NiGa_2O_4$ compound. Likewise, Ni^{2+} ions (majority) and Ni^{3+} ions (minority) were observed in the Ni K-edge XANES. The Ni^{2+} ions may provide NiO-type antiferromagnetic ordering in the sample. However, the Ni^{3+} ions with $3d^7$ electronic configuration may contribute to the paramagnetic character of the $NiGa_2O_4$ compound. The magnetic characterization of $NiGa_2O_4$ is less explored in the literature. Therefore, further theoretical and experimental studies are needed to confirm the origin of magnetism in $NiGa_2O_4$. It is seen in Fig. 6 that the magnetization is decreased at 300 K. The magnetization can randomly flip direction under the influence of temperature.[28] At low temperatures, the thermal agitation is minimized and the degree of alignment of the atomic magnetic moments is the greatest. At high temperatures, abundant thermal agitation leads to a decrease in the alignment of the atomic magnetic moments, and consequently the magnetization decreases.

Conclusions

A $NiGa_2O_4$ compound is prepared using a sonication-assisted chemical preparation method and subsequent annealing at 1150°C. Rietveld refinement is performed on the XRD patterns and confirmed the single-phase nature with lattice parameters of $a = b =$ c= 8.2589 Å and $\alpha = \beta = \gamma = 90°$. The bandgap energy of the $NiGa_2O_4$ compound is ~4.1 eV. The O K-edge, Ni K-edge, and Ga K-edge XANES results confirm the Ni^{2+}/Ni^{3+} ions and Ga^{3+} ion in the $NiGa_2O_4$ compound. Magnetic studies (at 50 K) confirm the paramagnetic character of the compound. The magnetization decreases at 300 K because of a decrease in the alignment of the atomic magnetic moments at higher temperature.

Acknowledgments Aditya Sharma is thankful to the Honourable Vice-Chancellor and Dean(s) of Manav Rachna University, Faridabad, for constant support and encouragement. Hyun-Joon Shin would like to acknowledge the support by Regional Innovation Strategy (RIS) through the National Research Foundation of Korea (NRF) funded by the ministry of education (2021RIS-001) and the support by the commercialization promotion agency for R&D outcomes grant funded by the Korean government, 2022, research equipment technician training program (2018R1A6A9056986).

Conflict of interest The authors declare that they have no conflict of interest.

References

1. X. Zhang and A. Zunger, *Adv. Funct. Mater.* 20, 1944 (2010).
2. V. Stevanovi, M. d'Avezac, and A. Zunger, *J. Am. Chem. Soc.* 133, 11649 (2011).
3. J.K. Yao, F. Ye, and P. Fan, *Opt. Mat. Exp.* 8, 3438 (2018).
4. Y. Chai, L. Li, J. Lu, D. Li, J. Shen, Y. Zhang, J. Liang, and X. Wang, *J. Cat.* 371, 144 (2019).
5. T. Zhou, S. Cao, R. Zhang, J. Tu, T. Fei, T. Zhang, and A.C.S. Appl, *Mater. Interfaces* 11, 28023 (2019).
6. R. Tiwari, M. De, H.S. Tewari, and S.K. Ghoshal, *Results Phys.* 16, 102916 (2020).
7. D. Errandonea, R.S. Kumar, F.J. Manjón, V.V. Ursaki, and E.V. Rusu, *Phy. Rev. B.* 79, 024103 (2009).
8. M.R. Suchomel, D.P. Shoemaker, and L. Ribaud, *Phys. Rev. B* 86, 054406 (2012).
9. H. St. C. O'Neil, A. Navrotsky, Am. Mineral., **68** (1983) 181.

10. E.J. Palin and R. Harrison, *J. Am. Mineral.* 92, 1334 (2007).
11. B.A. Scott, K.H. Nichols, R.M. Potemski, and J.M. Woodall, *Appl. Phys. Lett.* 21, 121 (1972).
12. Z. Yu, H. Chen, Z. Li, Z. Yang, H. Song, Y. Gao, Y. Zhang, Y. Jin, Z. Jiao, M. Gong, J. Zhu, and X. Sun, *Mater. Lett.* 63, 37 (2009).
13. T. Suzuki, G.S. Murugan, and Y. Ohishi, *J. Lumin.* 113, 265 (2005).
14. L. Chen, T. Horiuchi, and T. Mori, *Appl. Catal. A: Gen.* 209, 97 (2001).
15. H. Xue, Z. Li, Z. Ding, L. Wu, X. Wang, and X. Fu, *Cryst. Growth Des.* 8, 4511 (2008).
16. X. Chu, J. Wang, L. Bai, Y. Dong, W. Sun, and W. Zhang, *Sens. Actuators B Chem.* 255, 2058 (2018).
17. S. Liu, K.S. Hui, K.N. Hui, H.-F. Li, K.W. Ng, J. Xu, Z. Tang, and S.C. Jun, *J. Mater. Chem. A Mater. Energy Sustain.* 5, 19046 (2017).
18. L. Ding, J. Yan, Z. Zhao, and D. Lic, Sens. Actuators: B. *Chemical* 296, 126705 (2019).
19. J. Shi, W. Yu, I. Bergmann, H. Bremers, V. Sepelák, W. Mader, and K.D. Becker, *J. Alloy. Comp.* 504S, S432 (2010).
20. H. Li, F. Qi, F. Yang, and Z. Sun, *J. Coll. Inter. Sci.* 587, 302 (2021).
21. A. Sharma, J.P. Singh, S.O. Won, K.H. Chae, S.K. Sharma, S. Kumar, in: S. Sharma (Ed.), Handbook of Materials Characterization, Springer, 2018, ISBN 978-3-319-92955-2, p. 497.
22. S. Layek and H.C. Verma, *J. Mag. Mag. Mat.* 397, 73 (2016).
23. J.G. Chen, *Surf. Sci. Rep.* 30, 1 (1997).
24. A. Sharma, M. Varshney, H.J. Shin, K.H. Chae, and S.O. Won, *RSC Adv.* 7, 52543 (2017).
25. N. Palina, L. Wang, S. Dash, X. Yu, M.B.H. Breese, J. Wang, and A. Rusydi, *Nanoscale* 9, 6094 (2017).
26. A. Sharma, M. Varshney, H. Saraswat, S. Chaudhary, J. Parkash, H.J. Shin, K.H. Chae, and S.O. Won, *Int. Nano Lett.* 10, 71 (2020).
27. K. Nishi, K.I. Shimizu, M. Tanamatsu, H. Yoshida, A. Satsuma, T. Tanaka, S. Yoshida, and T. Hattori, *J. Phys. Chem. B* 102, 10190 (1998).
28. A. Sharma, M. Varshney, Y. Kumar, B.H. Lee, S.O. Won, K.H. Chae, A. Vij, R.K. Sharma, and H.J. Shin, *J. Phys. Chem. Sol.* 161, 110476 (2022).